Journal of Hydrology 585 (2020) 124744

Contents lists available at ScienceDirect

Journal of Hydrology

journal homepage: www.elsevier.com/locate/jhydrol

Research papers

Spatiotemporal dynamics of soil moisture in the karst areas of China based on reanalysis and observations data

Yuanhong Deng[a,b,c], Shijie Wang[a,d], Xiaoyong Bai[a,e,f,*], Guangjie Luo[f], Luhua Wu[a,c], Fei Chen[a,g], Jinfeng Wang[a,g], Qin Li[a,c], Chaojun Li[a,h], Yujie Yang[a,h], Zeyin Hu[a,c], Shiqi Tian[a,h]

[a] State Key Laboratory of Environmental Geochemistry, Institute of Geochemistry, Chinese Academy of Sciences, Guiyang 550081, China
[b] Center for Lunar and Planetary Sciences, Institute of Geochemistry, Chinese Academy of Sciences, Guiyang 550081, China
[c] University of Chinese Academy of Sciences, Beijing 100049, China
[d] Puding Karst Ecosystem Observation and Research Station, Chinese Academy of Sciences, Puding 562100, China
[e] CAS Center for Excellence in Quaternary Science and Global Change, Xi'an 710061, Shanxi Province, China
[f] Guizhou Provincial Key Laboratory of Geographic State Monitoring of Watershed, Guizhou Education University, Guiyang 550018, China
[g] College of Resources and Environmental Engineering, Guizhou University, Guiyang 550025, China
[h] School of Geography and Environmental Sciences, Guizhou Normal University, Guiyang 550001, Guizhou Province, China

ARTICLE INFO

This manuscript was handled by C. Corradini, Editor-in-Chief, with the assistance of Stephen Worthington, Associate Editor

Keywords:
Karst
Soil moisture
China
Climate
NDVI
Sensitivity analysis

ABSTRACT

Soil moisture is one of the restricting factors in a fragile karst ecological environment. However, its spatiotemporal evolution characteristics in the karst areas of China remain poorly understood. Thus, based on soil moisture from reanalysis (ERA-Interim product) and ground stations, this study used the Mann-Kendall test, the Theil-Sen slope estimator, sensitivity analysis and stepwise regression and obtained the following results: 1) ERA-Interim soil moisture well reflected the interannual change of observational soil moisture at 0–7, 7–28 and 28–100 cm. 2) The reanalysis and station data showed that soil at various depths in the karst areas was dominated by a drying trend in 1982–2015. 3) Soil moisture in karst areas of southern China was high but decreased fastest. In the karst areas of northern China, soil moisture was low and declined quickly. Nevertheless, soil wetting was observed in the central karst areas of Qinghai-Tibet Plateau. 4) Changes of soil moisture throughout the karst region of China and its subareas were mainly affected by precipitation, followed by temperature. 5) In Qinghai-Tibet Plateau and southern China, soil moisture in karst areas is overall higher than that in non-karst areas when under low vegetation coverage levels (NDVI $\leq$ 0.3) of some climate zones, possibly caused by the centralized allocation of precipitation in karst areas due to exposed rocks. In conclusion, climate, vegetation, and geological background make the spatiotemporal distributions of soil moisture differ within the karst region, while the soil drying trend in recent decades and global climate change are not conducive to the ecological restoration of vulnerable karst areas.

1. Introduction

Soil moisture (SM) is one of the important components of soil that affects crop growth, vegetation distribution pattern, and soil microbial activities (Dunn et al., 1985; Moyano et al., 2013; Xia and Shao, 2008). The migration of soil matter (Stielstra et al., 2015) and the absorption and decomposition of terrestrial carbon are inseparable from the role of SM (Green et al., 2019). Besides, SM functions as the link between surface water and groundwater. The dynamics of SM influence surface energy allocation, evapotranspiration processes and are important for research on hydrological processes and climate prediction (Deng, 2020; Wang, 2018). To date, international research on the spatiotemporal dynamics of SM has focused on surface soil at a global scale (McColl et al., 2017a,b; Sheffield and Wood, 2008), particularly under the condition of global warming (Dai, 2013). Knowledge gaps exist in China's karst region where SM is a limiting factor in the ecological restoration of soil and plant. The shortage of soil water resources seriously impacts the local ecological environment and agricultural production (Qin et al., 2015).

Karst is a unique combination of aboveground and underground geomorphology produced by the water-chemical dissolution of soluble rocks, such as carbonate rocks, and is generally characterized by barren

* Corresponding author at: State Key Laboratory of Environmental Geochemistry, Institute of Geochemistry, Chinese Academy of Sciences. 99 Lincheng West Road, Guiyang 550081, Guizhou Province, China.
E-mail address: baixiaoyong@vip.skleg.cn (X. Bai).

https://doi.org/10.1016/j.jhydrol.2020.124744
Received 10 December 2019; Received in revised form 19 January 2020; Accepted 19 February 2020
Available online 20 February 2020

and rocky grounds, caves, and sinkholes (Li, 2018; Parise et al., 2015). Under the special geological background, karst possesses surface and underground water systems, which are connected by hydraulic connection as a whole, and with considerable surface water seepage, its hydrological characteristics are different from these of non-karst areas (Bailly-Comte et al., 2009). Ecosystem in a typical karst region is weakly resistant to external disturbances (Bai et al., 2013), particularly in the karst areas of southwestern China (Tian et al., 2016). In these areas, soil erosion is severe, soil thin, and vegetation coverage low (Febles et al., 2009), thereby resulting in a fragile soil environment and frequent temporary droughts (Deng, 2018; Ge and Wang, 2008). Previous studies have suggested that SM is a major constraint factor in karst ecosystems, and the role of SM in facilitating the ecological restoration and agricultural industrialization in the karst area has been investigated (Hartmann et al., 2014). Current research focuses on the spatial characteristics of SM in karst areas. Chen et al. (2010) studied the distribution differences of SM under different land use in a karst slope; Li et al. (2014) revealed the influence of rock exposure on the spatial distribution of SM; Liu et al. (2017) analyzed the spatial movement characteristics of SM on the grass slope of a karst peak-cluster area. However, without comparing with results from non-karst areas, it is unclear whether SM in karst areas has unique characteristics. Furthermore, a few studies about the trend of SM change in karst areas are primarily carried out on the scales of slope and small watershed (Chen et al., 2010; Fu et al., 2016). The geological-hydrological background of karst, such as slow soil formation rate and space mismatch between water and soil, leads to the strong spatial heterogeneity of SM (Li et al., 2014; McCole and Stern, 2007). Consequently, the conclusions of these previous studies are uncertain in large-scale karst areas. In addition, the interannual variation of SM is affected by various factors, including temperature, precipitation, and vegetation. The effects of these factors on SM vary under different spatiotemporal circumstances. Many scholars found that recent rising in global temperature was the dominant factor causing global soil drying (Dai, 2013; Feng and Fu, 2013), that precipitation controlled the drying trend of SM from 1979 to 2010 in China (Jia et al., 2018), and that vegetation restoration brought about the decline of SM in the Loess Plateau of China (Su and Shangguan, 2019). Therefore, it's necessary to study the effects of climate and vegetation on SM change in karst areas, promoting water and soil conservation and ecological restoration.

Here, this paper aims to explore the spatial and temporal characteristics of SM in the karst areas of China in 1982–2015. The concrete objectives are as follows: 1) evaluate the reliability of SM from reanalysis product (ERA-Interim) at different depths; 2) reveal the spatial distributions and change trends of SM in the karst region of China by using reanalysis and observations data; 3) analyze the effects of the normalized difference vegetation index (NDVI), precipitation, and temperature on SM based on sensitivity analysis and stepwise regression; and 4) discover SM differences between karst and non-karst areas in China.

2. Data and methods

2.1. Data and preprocessing

SM product from ERA-Interim reanalysis was provided by the European Center for Medium-Range Weather Forecasts (ECMWF) with spatial and temporal resolutions of 0.125° and monthly, respectively (https://www.ecmwf.int/), which has four SM layers (0–7, 7–28, 28–100, and 100–289 cm). The product was previously applied to the analysis of spatiotemporal changes in SM, hydrometeorology, and numerical simulation (Deng, 2020; Materia, 2014; Xia, 2014). Also, ERA-Interim reanalysis data included precipitation and temperature data with the same spatial and temporal resolutions as the SM product. The observational SM data were obtained from the International Soil Moisture Network (ISMN), which collects free and high-quality in-situ

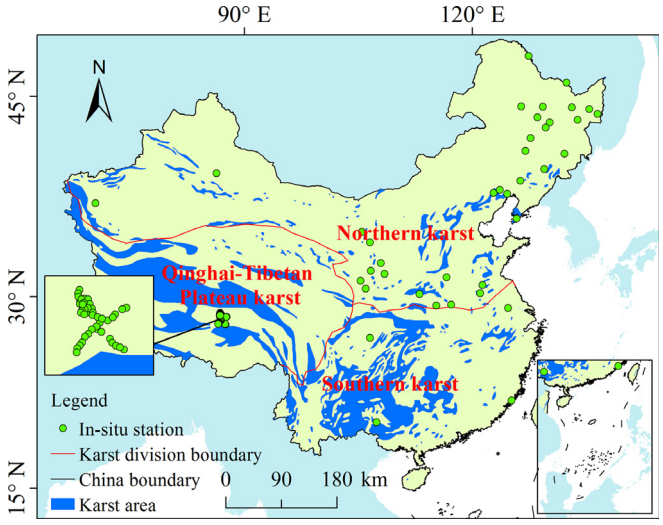

Fig. 1. Spatial distributions of karst areas and SM ground stations in China.

SM data worldwide (http://www.ipf.tuwien.ac.at/) (Dorigo et al., 2011). However, the temporal resolution and time length of observation stations vary (Deng et al., 2019). GIMMS NDVI3g (1982–2015) (https://ecocast.arc.nasa.gov/data/pub/gimms/), with spatial and temporal resolutions of 8 km and 15 days, respectively, was also used in this study (Yang et al., 2019).

The actual soil thickness in typical karst areas is usually less than 1 m. Therefore, SM product and site-measured data at 0–7, 7–28, and 28–100 cm were used in this study. Temporal resolutions of SM, precipitation, temperature and NDVI data were converted to the annual scale, and among them, spatial resolutions of gridded data were interpolated to 0.125°. The time coverage for observational SM in China from ISMN was mostly 1981–1999, 2010–2016, and 2008–2010, with the monitoring times typically on the 8th, 18th, and 28th of each month. Thus, stations with observation duration less than 5 years were deleted to maintain a sufficient sample. The spatial distributions of all stations applied to evaluate ERA-Interim SM on the annual scale are shown in Fig. 1. Among them, 37 stations (Fig. S1), including four stations (BAISE, ZHUMADIA, XUZHOU, JIANPIN) located in karst region, were selected to analyze the temporal and spatial evolution of SM in view of their longer observation duration (1981–1999) and more observational data in vertical profile, with 11 layers, 1 (0–0.05 m), 2 (0.05–0.1 m), 3 (0.1–0.2 m), 4 (0.2–0.3 m), 5 (0.3–0.4 m), 6 (0.4–0.5 m), 7 (0.5–0.6 m), 8 (0.6–0.7 m), 9 (0.7–0.8 m), 10 (0.8–0.9 m), 11 (0.9–1 m). The nearest neighbor interpolation method was used to spatially match the ERA-Interim SM with the station data (Deng et al., 2019).

2.2. Study area

The distribution area of karst in China is 3.44 million km^2 (including the karst buried under nonsoluble rocks), which exceeds 1/3 of China's total land area. The exposed carbonate area of China's total land area is approximately 907,000 km^2, which accounts for approximately 1/7 of China's total land area. Eight provinces with Guizhou at the center comprise one of the largest concentrated karst districts in the world (Song et al., 2016). The thin soil layer and poor soil water retention capacity in karst areas result in a vulnerable soil ecosystem and low land productivity (Wang et al., 2004). The karst can be divided into exposed, covered and buried types in terms of rocks' distribution. The exposed type of China was used in this study (Fig. 1). In the exposed karst areas, the average annual precipitation and temperature are 24.7–2362.2 mm and − 25.2 °C – 24.8 °C, respectively, and the average elevation is 2887 m. The exposed karst areas of China (K) can be further

classified into three subareas: the karst of southern China (SK), the karst of northern China (NK), and the karst of Qinghai-Tibet Plateau (QK) (Jiang et al., 2011). SK primarily covers the tropical monsoon climate and the subtropical monsoon climate, which are wet, hot, and rainy (annual average temperature: > 15 °C; average annual precipitation: > 1000 mm), with typical karst developing. The climate in NK is dry and cool (average annual precipitation: < 800 mm), with considerable water and heat differences within the area. NK mostly covers temperate and western dry karst. QK has an average elevation of over 4000 m in an alpine cold region. The geographic environment of the Qinghai-Tibet Plateau plays an important role in weather and climate change in the Asian continent, and the plateau is a hotspot for research on global change (Boos and Kuang, 2010; Dong et al., 2016; Li et al., 2017).

2.3. Methods

Statistical indicators, correlation coefficient and bias, were used to evaluate ERA-Interim SM data (Kuriqi, 2016; Muceku et al., 2016). To reduce the effects of outliers on trend analysis, the Mann-Kendall (MK) nonparametric trend test and the Theil-Sen nonparametric linear trend estimator were combined to calculate the variation trends of SM, precipitation, temperature, and NDVI at the pixel and station scales (Tian et al., 2017). Unary linear regression was used for the trends of the aforementioned factors at the average regional scale as well as sensitivity analysis of SM to climate and vegetation (Albano et al., 2019). Furthermore, stepwise regression was adopted to determine the action intensity of precipitation, temperature, and NDVI on SM changes. The critical probability values of the introduced and culling variables were 0.05 and 0.1, respectively. To eliminate dimensional influence, the input data of stepwise regression at the pixel and regional average scales were standardized using standard deviation. Then, the standardized regression coefficients were obtained, the magnitude of which reflected the effect intensity of the corresponding variable on SM (Zhang et al., 2015). Specific research objectives and methods can be seen in the technical roadmap (Fig. S2).

3. Results

3.1. Evaluation of the ERA-Interim SM product

The in-situ SM from over 75% of stations (with the correlation significance level of 0.05) correlated well with the ERA-Interim product at each soil layer (Fig. 2a). From the surface to the deep layer, the average correlation coefficients were 0.77, 0.71, and 0.56, indicating that the ERA-Interim SM product can display the interannual change of actual SM. However, the correlation of the SM product weakened as depth increased. Notably, SM of a few stations significantly and negatively correlated with the ERA-Interim SM at 28–100 cm (Fig. 2a). In Fig. 2b, the deviation values of the ERA-Interim product from the in-situ observed data decreased as soil depth increased, with average biases of 0.037, 0.009, and −0.006 m^3/m^3, thereby suggesting that in terms of magnitude, the ERA-Interim SM overestimated the measured values at 0–7 cm and 7–28 cm and slightly underestimated at 28–100 cm. The aforementioned findings prove that the ERA-Interim SM product can well reflect the true state of SM from stations at the annual scale.

3.2. Spatiotemporal dynamics of SM in karst areas

3.2.1. Spatial distribution characteristics

At the multi-year average state, SM in China's karst areas decreases from southeast to northwest in space (Fig. 3a–c). Concerning the regional average (Fig. 3d), SM in SK is the highest, followed by that in QK. SM in NK is the lowest and less than the average SM in the entire karst region of China. From 0–7 to 28–100 cm, the spatial distribution patterns of SM are similar. But, the average SM of the entire karst region and its subareas slightly rises as soil depth increases. The in-situ observational SM shows more detailed characteristics on the vertical soil profile. The multi-year average SM of most stations, including stations in the karst area, grows with the increase of soil depth (Fig. 4), indicating that the vertical characteristics of SM from ERA-interim are consistent with that of the measured data.

3.2.2. Characteristics of change trend

The average SM time series in the karst region and its subareas decreased in 1982–2015 with some fluctuations, except for SM at deep depth in QK (Fig. S3). In particular, Table 1 shows that the reduction trends of the entire karst area, SK, and NK are significant, approximately −0.327 to −0.157 × 10^{-3} m^3/m^3 yr^{-1}. However, R^2 values, the goodness of fit, were below 0.5. SM in QK decreased insignificantly at 0–7 and 7–28 cm, and increased insignificantly at 28–100 cm. Simultaneously, as soil depth increased, the drying rates of SM in the entire karst region, NK, and QK slowed down. This phenomenon is probably because shallow SM is most directly affected by external factors, such as temperature and precipitation. Conversely, the drying trend of SM in SK accelerated in deeper soil depth.

The pixel-by-pixel SM change rate demonstrates that over 64% of soil-drying areas exist in the entire karst region at all depths (Fig. 5), with significant drying (*Z value* ≤ −1.96) of approximately 35% (Fig. S4); the soil-drying areas shrink from the surface to the deep soil. Remarkably, the spatial distribution of SM changes exhibited regional differences. Soil in over 58% of QK got wetting, mostly located at the center of QK, and in deeper soil layers, the soil-wetting areas and the average wetting rate increased slightly, which may be induced by the

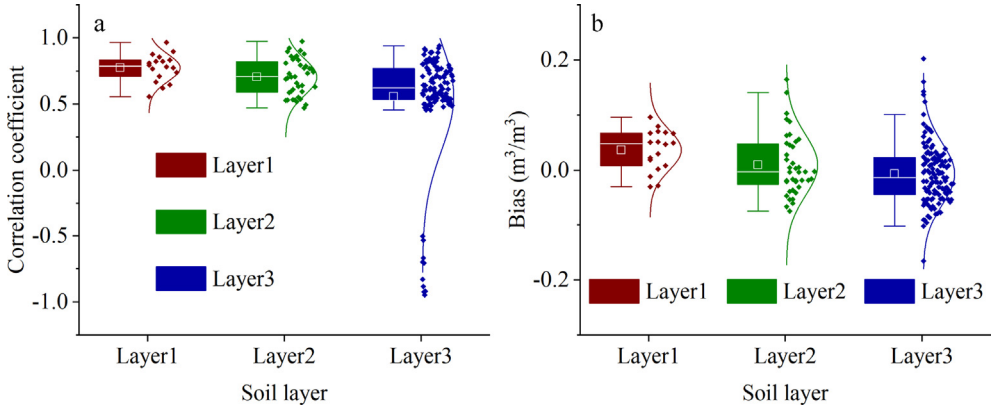

Fig. 2. Box plots for correlation coefficient (a) and bias (b) between the ERA-Interim SM product and in-situ SM at different depths. Fig. 2 show the 25th, 50th, and 75th percentiles and the average as well as the scatter and distribution curve. Layer1-3 mean soil depths, 0–7, 7–28 and 28–100 cm, respectively.

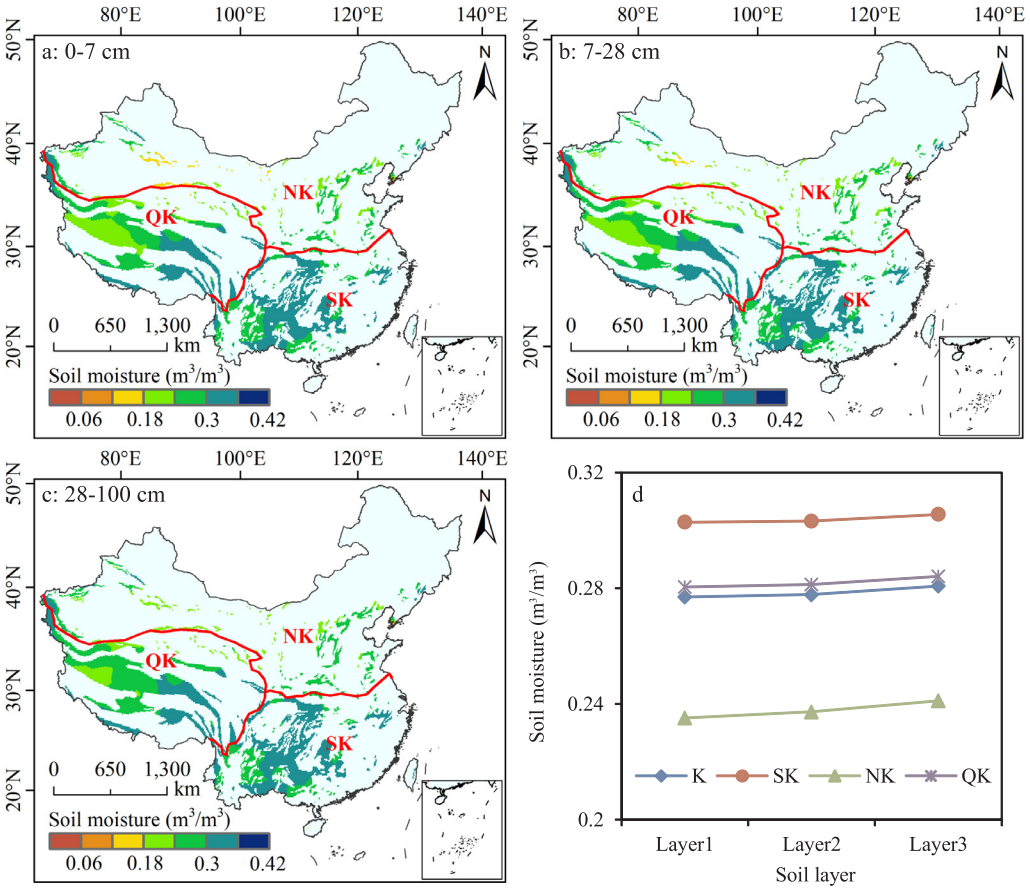

Fig. 3. Spatial distributions of the multi-year average SM in the karst areas (a–c) and the regional average SM (d). In Fig. 3, Layer 1–3 represent 0–7, 7–28, and 28–100 cm, respectively.

melting of deep frozen soil in the plateau due to the temperature rising. The regional mean values of SM change rates in Fig. 5d are consistent with the results presented in Table 1. Most of observational data, primarily in 1981–1999, showed decreasing trends (Fig. 6); also, SM at different soil depths from stations in karst areas decreased, except Xuzhou station.

3.3. Sensitivity of SM to climate and vegetation

The regression coefficient of SM and single influencing factor was regarded as the sensitivity coefficient (Table S1), the average SM in the karst region of China significantly showed negative sensitivity to the

Table 1
Linear trends of average SM in the karst region and its subareas from 1982 to 2015. The unit of slope in Table 1 is m^3/m^3 yr^{-1}.

Region	0–7 cm		7–28 cm		28–100 cm	
	Slope	R^2	Slope	R^2	Slope	R^2
K	−0.253**	0.24	−0.213**	0.21	−0.157*	0.16
SK	−0.320**	0.27	−0.323**	0.28	−0.327***	0.30
NK	−0.282**	0.27	−0.226**	0.23	−0.175**	0.20
QK	−0.136	0.04	−0.081	0.02	0.016	0.00

*, **, *** indicate significance at $p \leq 0.05$, $p \leq 0.01$, $p \leq 0.001$, respectively.

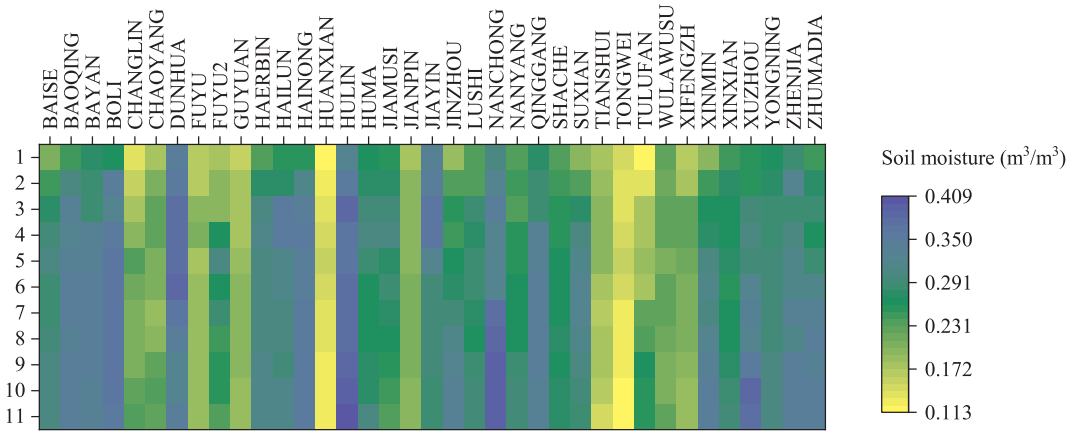

Fig. 4. Multi-year average SM from stations in China at different soil depths.

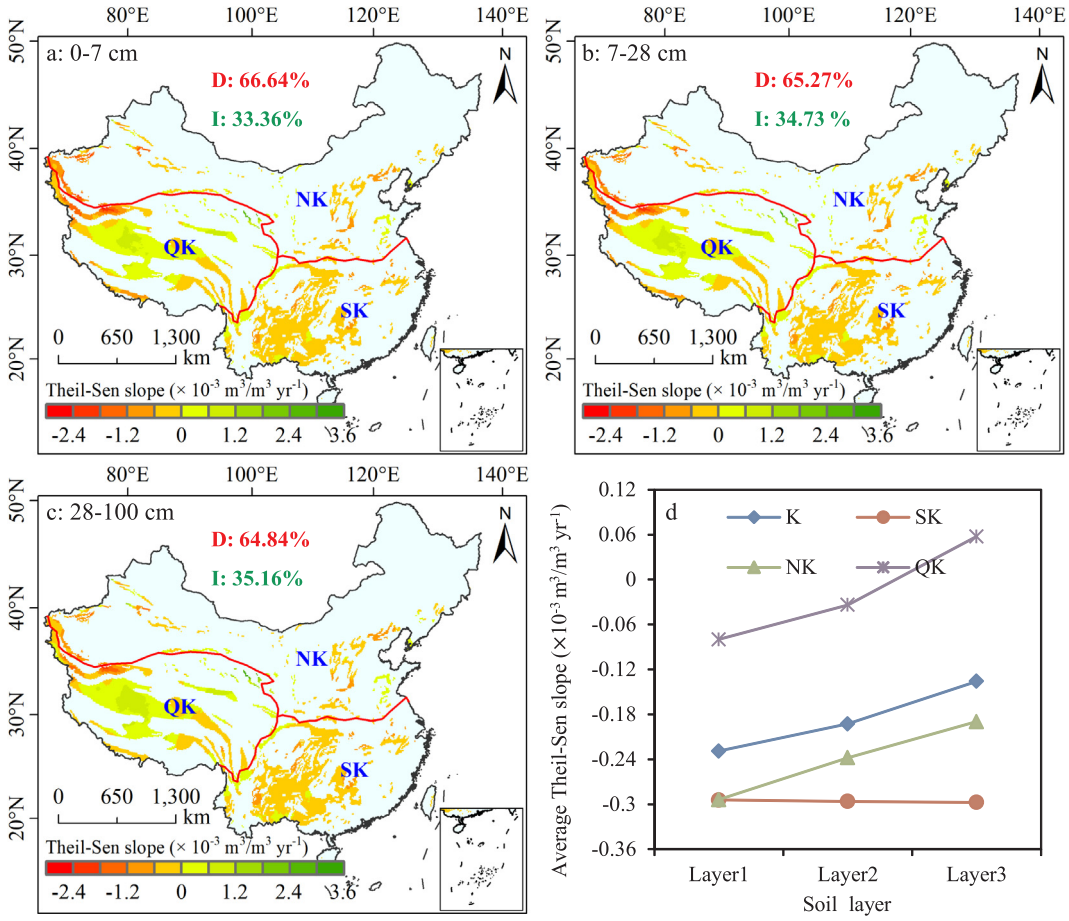

Fig. 5. Spatial distributions of SM trends from 1982 to 2015 in the karst region (a–c) and regional average values of SM trends (d). In Fig. 5a–c, D in red and I in green denote SM decreases and increases, respectively. (For interpretation of the references to colour in this figure legend, the reader is referred to the web version of this article.)

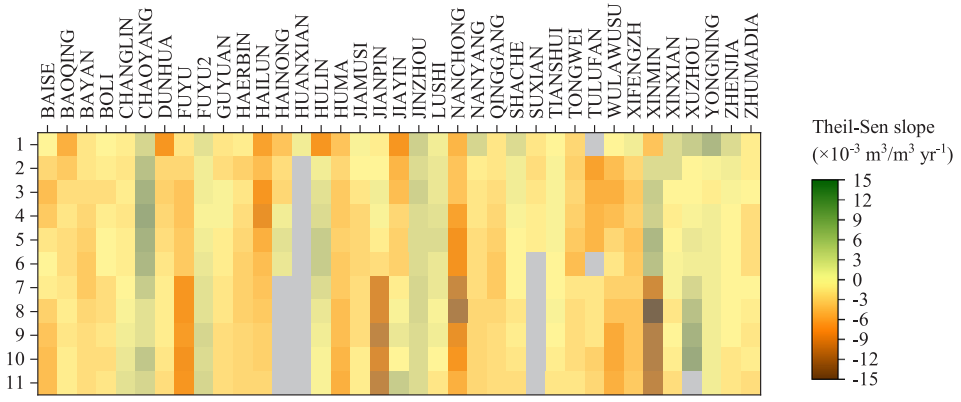

Fig. 6. Theil-Sen slope of SM from stations in China at different depths. *Note:* the observation period of most stations is in 1981–1999. The gray grid indicates that the station has data missing for more than one year at the soil depth.

average NDVI and positive sensitivity to the average annual precipitation in 1982–2015. Sensitivity of SM to vegetation or precipitation varied in karst subareas. Concretely, the average SM in NK exhibited the strongest negative sensitivity to vegetation, and the SM at 0–7 cm decreased by 0.03 m^3/m^3 every 0.01 increase of NDVI. The average SM in QK had a weak positive sensitivity to NDVI, and the average SM in SK performed the weakest sensitivity to precipitation. During the study period, the average SM in the karst region and its subareas showed extremely similar negative sensitivity to temperature (-0.005 m^3/m^3 $°C^{-1}$). With soil depth increasing, the sensitivities of the average SM to climate and vegetation in the karst region and its subareas weakened, except for the sensitivity of average SM to vegetation in QK. Spatial distribution for sensitivities of surface SM to climate and vegetation in Fig. 7 demonstrated that SM in the whole karst region was negatively sensitive to vegetation, mainly located in SK; however, varying from results in Table S1, the stronger positive or negative sensitivity was largely distributed in QK, the alpine karst area. The sensitivity of SM to precipitation was mainly positive, with it in QK the strongest and SK the weakest. The sensitivity of SM to temperature was mostly negative and differ slightly in space. Additionally, with the growth of soil depth, the

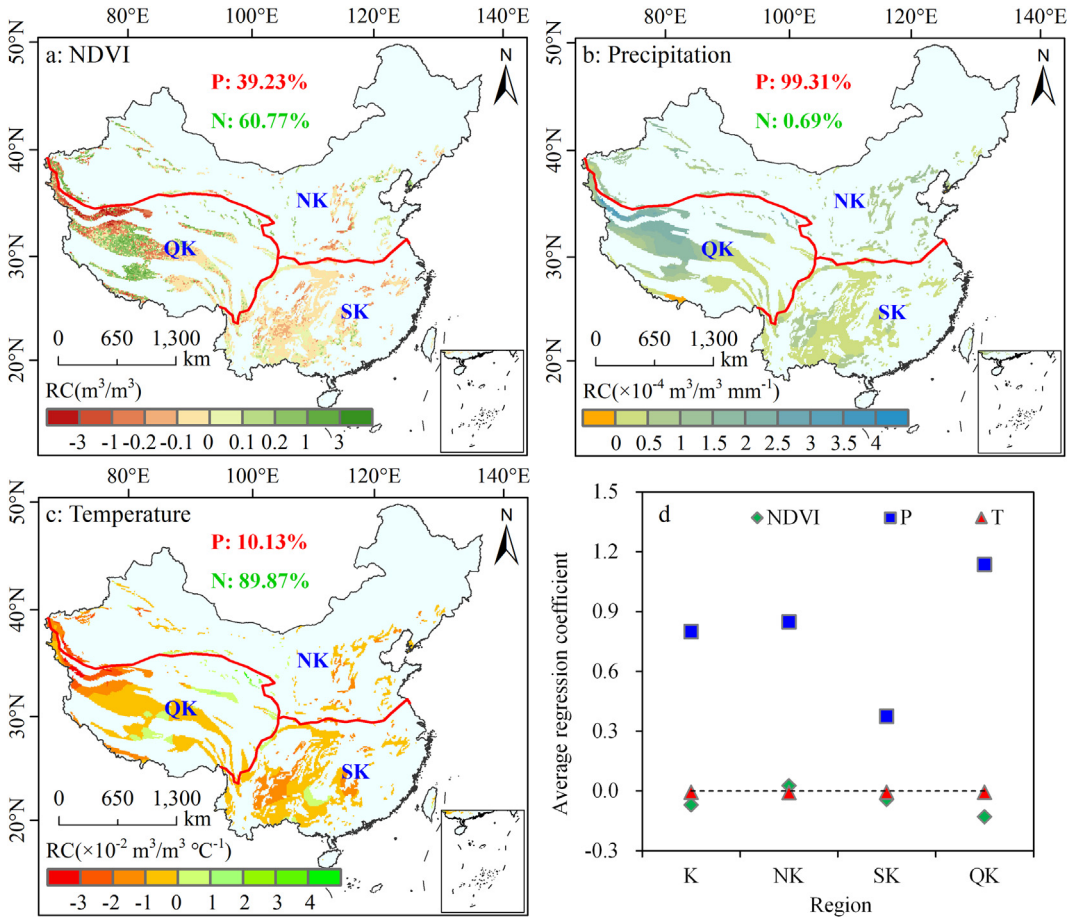

Fig. 7. Spatial distributions (a–c) and statistical analysis (d) of sensitivities of SM at 0–7 cm to NDVI, precipitation, and temperature in karst areas. RC represents regression coefficient. In Fig. 7a–c, P in red and N in green denote positive and negative sensitivity, respectively. P and T in Fig. 7d represent precipitation and temperature, respectively, and units of the average regression coefficient for NDVI, precipitation, temperature are m^3/m^3, 10^{-4} m^3/m^3 mm^{-1} and 10^{-2} m^3/m^3 $°C^{-1}$. (For interpretation of the references to colour in this figure legend, the reader is referred to the web version of this article.)

sensitivity diminished. It may result from the fact that in deeper soil, the SM is less disturbed by the external climate activities (McColl et al., 2017a).

4. Discussion

4.1. Spatiotemporal characteristics of SM in karst areas

The reanalysis and observational data demonstrated that the multi-year average SM of karst areas and non-karst areas had the same characteristics in the vertical profile (Figs. 5 and 6), that is, with the increase of depth, the SM generally increased. Differently, the average values of SM in the karst region and its subareas were higher than those in non-karst region and its corresponding subareas (Table S3), possibly caused by excessive coverage of arid areas in non-karst areas. However, compared with non-karst areas, typical karst areas are characterized by large ratio of rock to soil, discontinuous soil distribution and strong spatial heterogeneity due to slow soil formation rate and severe soil erosion, then influencing the allocation of precipitation, the process of runoff generation and confluence in karst areas, and the movement and distribution of SM (Chan, 2012; Zhang et al., 2008). Wang et al. (2016) proposed that in the karst areas, after the confluence of precipitation, rock outcrops distributed almost 50% of the runoff to the adjacent soil, which resulted in high SM between the rock outcrops. Climate is an important factor affecting SM (Deng et al., 2020) and NDVI can approximately indicate the land surface coverage and rocky desertification (Chen et al., 2019). Hence, to reduce the large divergence of climate between karst and non-karst regions in China, this study preliminarily compared SM under different vegetation coverage levels of each climate zone for the karst and non-karst areas in southern China and Qinghai-Tibet Plateau. According to UNEP (1997), the climate zones were obtained by dividing aridity index (http://www.cgiar-csi.org) into five zones (Fig. S1), including HA (Hyper Arid), A (Arid), SA (Semi-Arid), DSH (Dry sub-humid) and H (Humid). Fig. 8 shows that in the southern of China, SM in the karst areas under some NDVI levels of the DSH and H climate zones is overall higher than that in the non-karst areas, although the results are opposite in the SA; meanwhile, with the increase of vegetation coverage, the divergence of SM between karst and non-karst areas decreases. In the Qinghai-Tibet Plateau, the SM in karst areas with low vegetation coverage levels (NDVI $\leq$ 0.3) is higher than that in non-karst areas. With vegetation cover improving to over 0.3, the SM in non-karst areas exceeds that in karst areas. Moreover, similar findings were also found in deeper SM (7–28 and 28–100 cm) (Table S4). The above results may result from the redistribution of rainfall by exposed rocks in karst areas on a macro scale. But, despite the more detailed division, the areas of the karst and non-karst under some vegetation classes of the same climate zone in southern China remain quite different (Table S5), and the relevant results from reanalysis data require further validation. More importantly, it is critical to compare SM between karst and non-karst areas by using sufficient SM stations with long observation time and even distributions.

In terms of change trend, the reanalysis and observational data show that the average SM of different depths in both the karst and non-karst regions of China declined (Figs. 5 and 6), which is consistent with

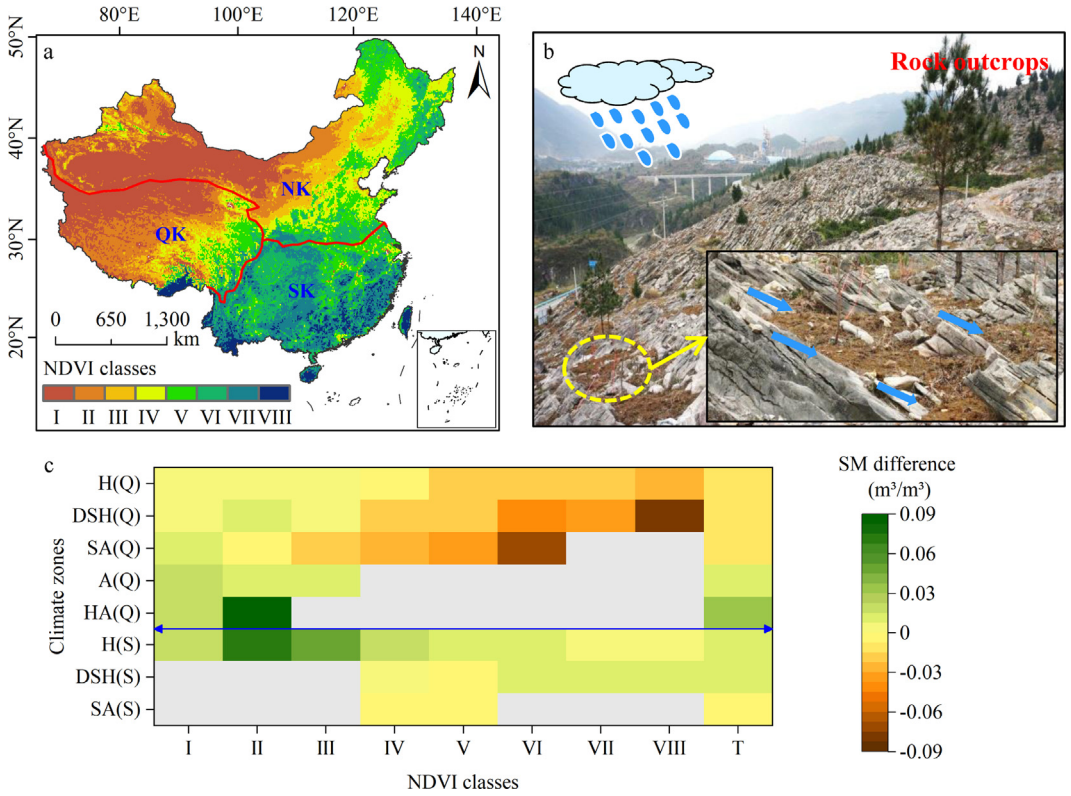

Fig. 8. Classification of NDVI in China (a), schematic diagram of precipitation distribution to soil by rock outcrops in the karst of southern China (b), and difference of multi-year average SM at 0–7 cm between karst and non-karst areas in Qinghai-Tibet Plateau and southern China under different NDVI classes of climate zones (c). In Fig. 8a, I, II, III, IV, V, VI, VII and VIII respectively represent NDVI classes of ≤0.1, 0.1–0.2, 0.2–0.3, 0.3–0.4, 0.4–0.5, 0.5–0.6, 0.6–0.7, > 0.7; In Fig. 8c, T represents that all NDVI classes are considered in the climate zone; Q and S represent Qinghai-Tibetan Plateau and southern China, respectively, distinguished by the blue double arrow line. The gray grid indicates no data. (For interpretation of the references to colour in this figure legend, the reader is referred to the web version of this article.)

the background that the global and China's SM has been decreasing in recent years (Dai, 2013; Feng and Fu, 2013; Jia et al., 2018). However, remarkable differences in SM among karst subareas in China are also observed. SM of SK is large, but the average SM has reduced fastest in the past 34 years, with the drying rate slightly increasing in deep soil; the SM in NK is low, but the soil drying trend is dominant in the area. During the study period, SM in half of QK raised, and the soil wetting areas expanded with the increase of soil depth. The above findings can be supported by the conclusions that SM in the eastern part of China decreased significantly from 1979 to 2010 (Chen et al., 2016) and that the remote sensing observation showed the wetting trend in the central part of the Qinghai-Tibet Plateau (van der Velde et al., 2014). Overall, as an ecologically fragile (Li et al., 2014; Parise et al., 2009) and sensitive region, karst presents the barren soil with poor water holding capacity and is easy to form a geological drought (Ni et al., 2009). Besides, the karst area with abundant precipitation is prone to soil erosion (Chen et al., 2019), which exacerbates the uneven distributions of local soil and water resources.

4.2. Causes of SM change under global warming

4.2.1. Changes of climate and vegetation in karst areas

In 1982–2015, the average temperature and NDVI of the karst region and its subareas exhibited increasing trends (Fig. S3), particularly in SK. Precipitation in the karst region, SK, and NK decreased, whereas that in QK experienced an increasing trend. Spatially (Figs. 9 and S4), vegetation in the karst region was dominated by greening, with the increasing areas accounting for 80.3% (55.53%, *Z value* ≥ 1.96). The greening area in each subarea exceeded 70%, but their greening rates differed. The average rate of NDVI trends in SK (1.41×10^{-3} yr^{-1}) was two times that in the entire karst region (0.66×10^{-3} yr^{-1}). For precipitation, the area ratio of increase to decrease over the karst areas was approximately 1:1, and the area proportions of significant increase and decrease were 19.97% and 7.73%, respectively. The areas with precipitation reduction were mostly distributed in NK as well as the northwestern and northern parts of SK. Precipitation in NK decreased the fastest. Precipitation in QK was dominated by increasing, which mostly occurred in the areas where SM increased. The temperature in 78.19% of the entire karst region significantly raised with an average temperature change rate of 0.29×10^{-3} °C yr^{-1} and the discrepancy between the average temperature change rates in the subareas was indistinctive.

4.2.2. Effects of NDVI, precipitation, and temperature on SM

Sensitivity analysis revealed that SM in karst areas related to vegetation and climate, but the relative importance of precipitation, temperature, and vegetation to SM changes has not been reflected. In this regard, combined with the changing trend of each factor, the stepwise regression results (Table 2) showed that over 70% of the average SM change in the entire karst region and SK was affected by precipitation increasing and temperature rising. SM change in all soil layers of NK was mostly affected by precipitation declining, with the interpretation degree ranging from 76% to 82%. In QK, 66% of SM change at 0–7 cm was affected by precipitation and temperature. However, 68% was mostly affected by precipitation, temperature, and NDVI at 7–28 cm, with the influence of temperature increasing, and SM change was primarily affected by precipitation at 28–100 cm. All the standardized regression coefficients indicate that the average SM in karst and its subareas is principally influenced by precipitation.

In Fig. 10, the absolute values and the covered space of the stepwise

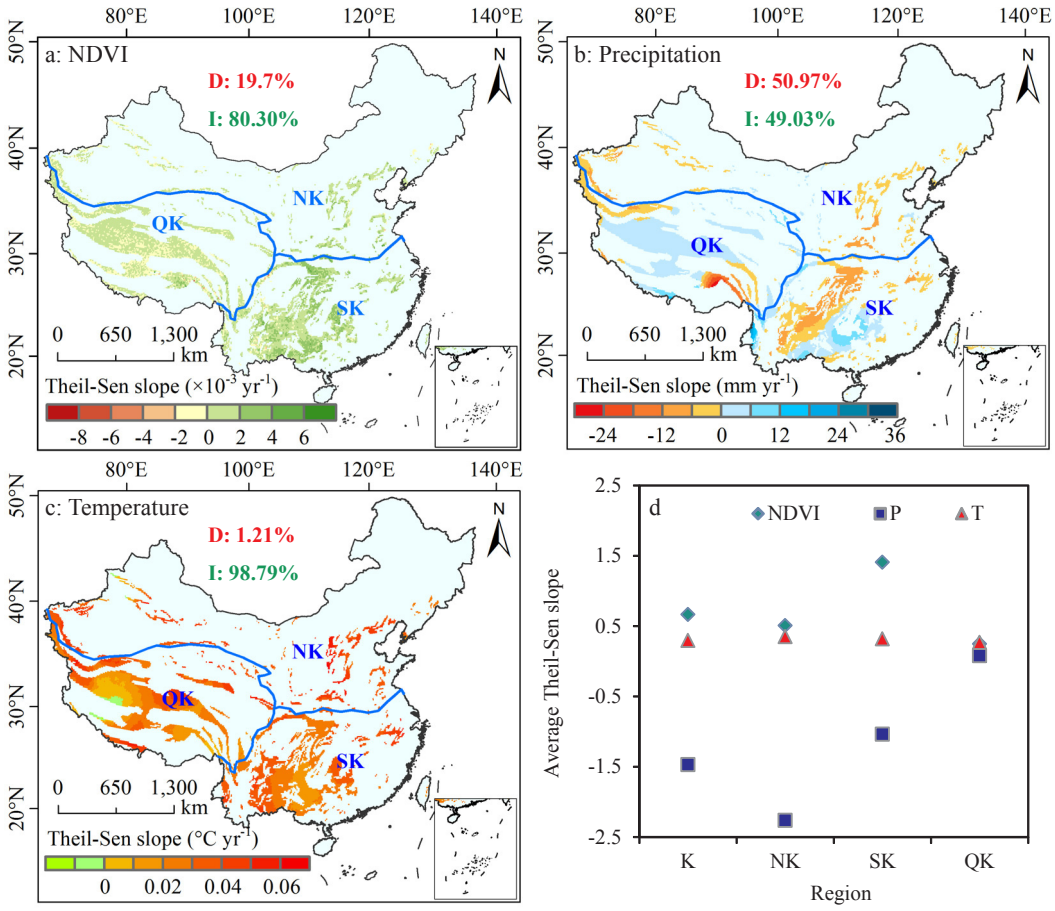

Fig. 9. Spatial distributions of the Theil-Sen slope for NDVI, precipitation, and temperature in the karst region (a–c) and the regional mean rates of change (d). In Fig. 9a–c, D in red and I in green denote decrease and increase, respectively. In Fig. 9d, P and T represent precipitation and temperature, respectively, and units of the average regression coefficient for NDVI, precipitation, temperature are m^3/m^3, 10^{-4} m^3/m^3 mm^{-1} and 10^{-2} m^3/m^3 $°C^{-1}$. (For interpretation of the references to colour in this figure legend, the reader is referred to the web version of this article.)

regression coefficients indicate that at the pixel scale, the surface SM in karst region and its subareas was dominantly affected by precipitation, followed by temperature. The area proportions of temperature and precipitation that affected surface SM were the largest in SK, and the greatest effect of NDVI on SM was distributed in NK. The mean interpretation power R^2 of the stepwise regression for SM at 0–7 cm was 0.71, with the interpretation power below 50% primarily distributed in QK, indicating that SM in QK was also affected by other factors, such as altitude (Cao et al., 2017) and human activities (Chaturvedi et al., 2017). In deeper soil (Figs. S5 and 6), the interpretation power of SM change in the karst region and its subareas diminished, particularly in QK.

Previous studies have found that temperature is a major contributor to global soil drying (Cheng and Huang, 2016; Feng and Fu, 2013). Nonetheless, in this study, the influence of precipitation on SM change at 0–7, 7–28, 28–100 cm is stronger than that of temperature. Specifically, the decrease of precipitation is the major cause of soil drying in the karst region of China, also true in SK. In QK, considerable differences are observed in the causes of SM change. Fig. 10 shows that the soil-wetting areas at 0–7 cm in QK are primarily affected by the increase in precipitation, and temperature warming does not have a positive effect on SM. The results conform to the finding that soil wetting in the early summer in the Qinghai-Tibet Plateau is driven by precipitation growth (Zhang et al., 2017). By contrast, the soil-drying areas in QK are mostly influenced by the decline in precipitation and the rising temperature. It may be attributed to global warming resulting in permafrost melting and soil water infiltration, thereby making the upper soil dry in the Qinghai-Tibet Plateau (Xue et al., 2009). In NK, the influence of vegetation on SM has elicited extensive concern, particularly in the Loess Plateau where afforestation caused local SM declining and forming dry soil layers (Jia et al., 2017); although compared with other karst subareas, SM of various soil depths in NK showed the most

Table 2
Stepwise regressions of SM and precipitation, temperature, and NDVI in the karst region and its subareas from 1982 to 2015. *Y*, *P*, and *T* in Table 2 represent soil moisture, precipitation, and temperature, respectively.

Soil depth	K	NK	SK	QK
0–7 cm	$Y = 0.792P - 0.295T$ $R^2 = 0.78$	$Y = 0.907P$ $R^2 = 0.82$	$Y = 0.849P - 0.405T$ $R^2 = 0.84$	$Y = 0.740P - 0.351T$ $R^2 = 0.66$
7–28 cm	$Y = 0.8P - 0.261T$ $R^2 = 0.77$	$Y = 0.907P$ $R^2 = 0.82$	$Y = 0.850P - 0.405T$ $R^2 = 0.84$	$Y = 0.698P - 0.484T + 0.299NDVI$ $R^2 = 0.68$
28–100 cm	$Y = 0.793P - 0.207T$ $R^2 = 0.72$	$Y = 0.872P$ $R^2 = 0.76$	$Y = 0.843P - 0.404T$ $R^2 = 0.82$	$Y = 0.733P$ $R^2 = 0.54$

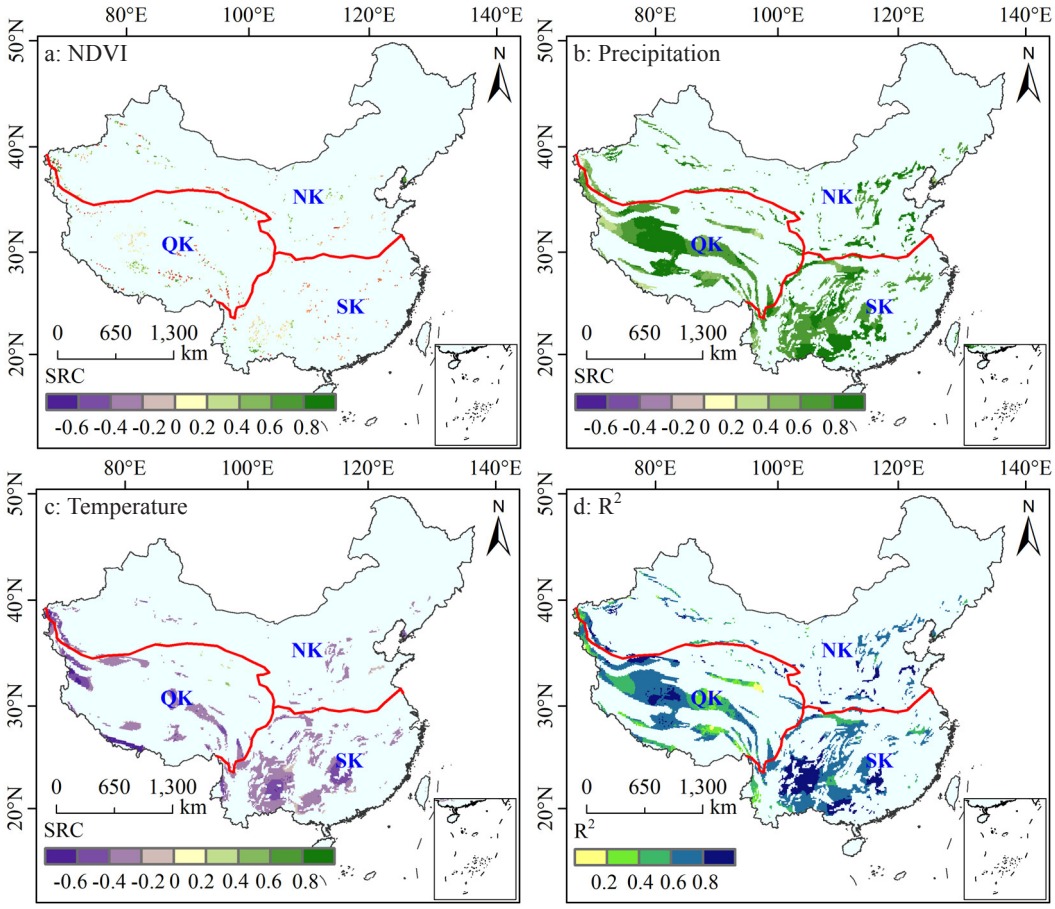

Fig. 10. Spatial distributions for standardization coefficients of NDVI (a), precipitation (b), and temperature (c) and explanatory strength R^2 (d) of stepwise regression for SM at 0–7 cm. In Fig. 10, SRC represents standardized regression coefficient.

significant negative sensitivity to NDVI, the soil drying trend was mainly controlled by precipitation. In summary, SM in the karst region of China went down under global climate change in 1982–2015, which is primarily endangered by reduced precipitation. The reduction in SM can hinder the natural growth of crops, boost the demand for agricultural irrigation, and increase the risk of drought. Therefore, effective SM management measures are necessary to avoid the risks and harm caused by soil drying in accordance with the actual situations in the karst areas of China.

5. Conclusion

SM plays an important role in ecological restoration and agricultural water resource management in karst areas. Combined the SM from reanalysis and station data with precipitation, temperature, and NDVI, this study found that climate, vegetation, and geological background made the spatiotemporal distributions of SM differ within the karst region, as follows:

1) ERA-Interim SM product reflected changes of in-situ observed SM well. However, the correlation weakened as depth increased, and in-situ SM was overestimated at 0–7 and 7–28 cm and slightly underestimated at 28–100 cm.
2) The trend analysis showed that SM in the entire karst region significantly decreased in 1982–2015, with over 64% areas drying at all soil layers.
3) SM in SK was the highest, but its drying speed was the fastest; SM in NK was lower than the average level in entire karst region and its decrease rate was higher than the average rate of the karst region, indicating that the risk of drought is possibly enhanced in SK and NK. In QK, the significant decrease of average SM was observed in the surface soil from 1982 to 2015, although over 58% soil-wetting area was observed.
4) Under the global change, the trends of SM in the entire karst region and its subareas were dominated by precipitation, followed by temperature. The average SM changes in the karst region and SK at all depths were mainly affected by precipitation increasing and temperature warming; SM changes in NK were mostly influenced by precipitation; factors that affected SM change in QK varied at different depths.
5) In southern China, the SM under some vegetation levels of DSH and H climate zones in karst areas is higher than that in non-karst areas. In the Qinghai-Tibet Plateau, within a climate zone, the SM at the lower vegetation coverage levels (NDVI less than 0.3) in karst areas generally exceeds that in non-karst areas with the results opposite as the NDVI increases to over 0.3. The findings may be the result that the rock outcrops in karst areas with low vegetation coverage lead to the redistribution of precipitation.

CRediT authorship contribution statement

Yuanhong Deng: Data curation, Formal analysis, Writing - original draft. **Shijie Wang:** Conceptualization, Supervision. **Xiaoyong Bai:** Conceptualization, Supervision. **Guangjie Luo:** Visualization. **Luhua Wu:** Visualization. **Fei Chen:** Visualization. **Jinfeng Wang:** Visualization. **Qin Li:** Visualization. **Chaojun Li:** Writing - review & editing. **Yujie Yang:** Writing - review & editing. **Zeyin Hu:** Writing - review & editing. **Shiqi Tian:** Writing - review & editing.

Declaration of Competing Interest

The authors declare that they have no known competing financial interests or personal relationships that could have appeared to influence the work reported in this paper.

Acknowledgments

We thank ECMWF (https://www.ecmwf.int/) for sharing SM products freely. The research was supported by the National key research program of China [grant numbers 2016YFC0502300, 2016YFC0502102], Strategic Priority Research Program of the Chinese Academy of Sciences [grant number XDA23060100], Western Light Talent Program (Category A) [grant number 2018-99], United fund of karst science research center [grant number U1612441], Science and Technology Plan of Guizhou Province of China [grant number 2017–2966].

Appendix A. Supplementary data

Supplementary data to this article can be found online at https://doi.org/10.1016/j.jhydrol.2020.124744.

References

Albano, C.M., et al., 2019. Spatial patterns of meadow sensitivities to interannual climate variability in the Sierra Nevada. Ecohydrology 12 (7). https://doi.org/10.1002/eco.2128.

Bai, X.Y., Wang, S.J., Xiong, K.N., 2013. Assessing spatial-temporal evolution processes of karst rocky desertification land: indications for restoration strategies. Land Degrad. Dev. 24 (1), 47–56. https://doi.org/10.1002/ldr.1102.

Bailly-Comte, V., Jourde, H., Pistre, S., 2009. Conceptualization and classification of groundwater-surface water hydrodynamic interactions in karst watersheds: case of the karst watershed of the Coulazou River (Southern France). J. Hydrol. 376 (3–4), 456–462. https://doi.org/10.1016/j.jhydrol.2009.07.053.

Boos, W.R., Kuang, Z., 2010. Dominant control of the South Asian monsoon by orographic insulation versus plateau heating. Nature 463 (7278), 218–U102. https://doi.org/10.1038/nature08707.

Cao, W., Sheng, Y., Wu, J.C., Li, J., 2017. Spatial variability and its main controlling factors of the permafrost soil-moisture on the northern-slope of Bayan Har Mountains in Qinghai-Tibet Plateau. J. Mount. Sci. 14 (12), 2406–2419. https://doi.org/10.1007/s11629-017-4467-z.

Chan, Y., et al., 2012. Hypolithic microbial communities: between a rock and a hard place. Environ. Microbiol. 14 (9), 2272–2282. https://doi.org/10.1111/j.1462-2920.2012.02821.x.

Chaturvedi, R.K., Raghubanshi, A.S., Tomlinson, K.W., Singh, J.S., 2017. Impacts of human disturbance in tropical dry forests increase with soil moisture stress. J. Veg. Sci. 28 (5), 997–1007. https://doi.org/10.1111/jvs.12547.

Chen, X., et al., 2016. Detecting significant decreasing trends of land surface soil moisture in eastern China during the past three decades (1979–2010). J. Geophys. Res.-Atmos. 121 (10), 5177–5192. https://doi.org/10.1002/2015jd024676.

Chen, F., et al., 2019. Assessing spatial-temporal evolution processes and driving forces of karst rocky desertification. Geocarto Int. https://doi.org/10.1080/10106049.2019.1595175.

Chen, H., Zhang, W., Wang, K., Fu, W., 2010. Soil moisture dynamics under different land uses on karst hillslope in northwest Guangxi, China. Environ. Earth Sci. 61 (6), 1105–1111. https://doi.org/10.1007/s12665-009-0428-3.

Cheng, S., Huang, J., 2016. Enhanced soil moisture drying in transitional regions under a warming climate. J. Geophys. Res.-Atmos. 121 (6), 2542–2555. https://doi.org/10.1002/2015jd024559.

Dai, A., 2013. Increasing drought under global warming in observations and models. Nat. Clim. Change 3 (1), 52–58. https://doi.org/10.1038/nclimate1633.

Deng, Y., et al., 2018. Relationship among land surface temperature and LUCC, NDVI in typical karst area. Sci. Rep. 8. https://doi.org/10.1038/s41598-017-19088-x.

Deng, Y., et al., 2019. Comparison of soil moisture products from microwave remote sensing, land model, and reanalysis using global ground observations. Hydrol. Process. https://doi.org/10.1002/hyp.13636.

Deng, Y., et al., 2020. Variation trend of global soil moisture and its cause analysis. Ecol. Indic. 110, 105939. https://doi.org/10.1016/j.ecolind.2019.105939.

Dong, W., et al., 2016. Summer rainfall over the southwestern Tibetan Plateau controlled by deep convection over the Indian subcontinent. Nat. Commun. 7. https://doi.org/10.1038/ncomms10925.

Dorigo, W.A., et al., 2011. The International Soil Moisture Network: a data hosting facility for global in situ soil moisture measurements. Hydrol. Earth Syst. Sci. 15 (5), 1675–1698. https://doi.org/10.5194/hess-15-1675-2011.

Dunn, P.H., Barro, S.C., Poth, M., 1985. Soil-moisture affects survival of microorganisms in heated chaparral soil. Soil Biol. Biochem. 17 (2), 143–148. https://doi.org/10.1016/0038-0717(85)90105-1.

Febles, J.M., Tolon, A., Vega, M.B., 2009. Edaphic indicators for assesment of soil erosion in karst regions, province of havana, cuba. Land Degrad. Dev. 20 (5), 522–534. https://doi.org/10.1002/ldr.929.

Feng, S., Fu, Q., 2013. Expansion of global drylands under a warming climate. Atmos. Chem. Phys. 13 (19), 10081–10094. https://doi.org/10.5194/acp-13-10081-2013.

Fu, T., Chen, H., Fu, Z., Wang, K., 2016. Surface soil water content and its controlling factors in a small karst catchment. Environ. Earth Sci. 75 (21). https://doi.org/10.1007/s12665-016-6222-0.

Ge, Y., Wang, S., 2008. Correlations between soil moisture and δ~(13)C value of plant leave under karst and non-karst backgrounds—a case study in Wangjiazhai basin, Qingzhen city, Guizhou province. Carsol. Sin. 27 (2), 108–114.

Green, J.K., et al., 2019. Large influence of soil moisture on long-term terrestrial carbon uptake. Nature 565 (7740). https://doi.org/10.1038/s41586-018-0848-x. 476-+.

Hartmann, A., Goldscheider, N., Wagener, T., Lange, J., Weiler, M., 2014. Karst water resources in a changing world: review of hydrological modeling approaches. Rev. Geophys. 52 (3), 218–242. https://doi.org/10.1002/2013rg000443.

Jia, B., Liu, J., Xie, Z., Shi, C., 2018. Interannual variations and trends in remotely sensed and modeled soil moisture in China. J. Hydrometeorol. 19 (5), 831–847. https://doi.org/10.1175/jhm-d-18-0003.1.

Jia, X., Shao, M.A., Zhu, Y., Luo, Y., 2017. Soil moisture decline due to afforestation across the Loess Plateau, China. J. Hydrol. 546, 113–122. https://doi.org/10.1016/j.jhydrol.2017.01.011.

Jiang, Z., et al., 2011. Calculation of atmospheric CO_2 sink formed in karst progresses of the karst divided regions in China. Carsol. Sin. 30 (4), 363–367.

Kuriqi, A., 2016. Assessment and quantification of meteorological data for implementation of weather radar in mountainous regions. Mausam 67 (4), 789–802.

Li, J., et al., 2017. Moisture increase in response to high-altitude warming evidenced by tree-rings on the southeastern Tibetan Plateau. Clim. Dyn. 48 (1–2), 649–660. https://doi.org/10.1007/s00382-016-3101-z.

Li, H., et al., 2018. Spatiotemporal distribution and national measurement of the global carbonate carbon sink. Sci. Total Environ. 643, 157–170. https://doi.org/10.1016/j.scitotenv.2018.06.196.

Li, S., Ren, H.D., Xue, L., Chang, J., Yao, X.H., 2014. Influence of bare rocks on surrounding soil moisture in the karst rocky desertification regions under drought conditions. Catena 116, 157–162. https://doi.org/10.1016/j.catena.2013.12.013.

Liu, W., Wang, S., Luo, W., Dai, W., Bai, E., 2017. Characteristics of soil water movement in a grass slope in a karst peak-cluster region, China. Hydrol. Process. 31 (6), 1331–1348. https://doi.org/10.1002/hyp.11105.

Materia, S., et al., 2014. Impact of atmosphere and land surface initial conditions on seasonal forecasts of global surface temperature. J. Clim. 27 (24), 9253–9271. https://doi.org/10.1175/jcli-d-14-00163.1.

McCole, A.A., Stern, L.A., 2007. Seasonal water use patterns of Juniperus ashei on the Edwards Plateau, Texas, based on stable isotopes in water. J. Hydrol. 342 (3–4), 238–248. https://doi.org/10.1016/j.jhydrol.2007.05.024.

McColl, K.A., et al., 2017a. The global distribution and dynamics of surface soil moisture. Nat. Geosci. 10 (2). https://doi.org/10.1038/ngeo2868. 100-+.

McColl, K.A., et al., 2017b. Global characterization of surface soil moisture drydowns. Geophys. Res. Lett. 44 (8), 3682–3690. https://doi.org/10.1002/2017gl072819.

Moyano, F.E., Manzoni, S., Chenu, C., 2013. Responses of soil heterotrophic respiration to moisture availability: an exploration of processes and models. Soil Biol. Biochem. 59, 72–85. https://doi.org/10.1016/j.soilbio.2013.01.002.

Muceku, Y., Korini, O., Kuriqi, A., 2016. Geotechnical analysis of hill's slopes areas in heritage town of Berati, Albania. Period. Polytech. Civ. Eng. 60 (1), 61–73. https://doi.org/10.3311/PPci.7752.

Ni, X.B., Liu, R.G., Wang, S.J., 2009. Remote sensing of land sensitivity to drought in the karst regions of southwest China. J. Southwest Univ. Nat. Sci. Ed. 31 (12), 140–144.

Parise, M., Closson, D., Gutierrez, F., Stevanovic, Z., 2015. Anticipating and managing engineering problems in the complex karst environment. Environ. Earth Sci. 74 (12), 7823–7835. https://doi.org/10.1007/s12665-015-4647-5.

Parise, M., De Waele, J., Gutierrez, F., 2009. Current perspectives on the environmental impacts and hazards in karst. Environ. Geol. 58 (2), 235–237. https://doi.org/10.1007/s00254-008-1608-2.

Qin, L., et al., 2015. Major problems and solutions on surface water resource utilisation in karst mountainous areas. Agric. Water Manage. 159, 55–65. https://doi.org/10.1016/j.agwat.2015.05.024.

Sheffield, J., Wood, E.F., 2008. Global trends and variability in soil moisture and drought characteristics, 1950–2000, from observation-driven Simulations of the terrestrial hydrologic cycle. J. Clim. 21 (3), 432–458. https://doi.org/10.1175/2007jcli1822.1.

Song, X., et al., 2016. Rock-weathering-related carbon sinks and associated ecosystem service functions in the karst critical zone in China. Acta Geogr. Sin. 71 (11), 1926–1938.

Stielstra, C.M., et al., 2015. Climatic and landscape influences on soil moisture are primary determinants of soil carbon fluxes in seasonally snow-covered forest ecosystems. Biogeochemistry 123 (3), 447–465. https://doi.org/10.1007/s10533-015-0078-3.

Su, B., Shangguan, Z., 2019. Decline in soil moisture due to vegetation restoration on the Loess Plateau of China. Land Degrad. Dev. 30 (3), 290–299. https://doi.org/10.1002/ldr.3223.

Tian, Y., Bai, X., Wang, S., Qin, L., Li, Y., 2017. Spatial-temporal changes of vegetation cover in Guizhou Province, Southern China. Chin. Geogr. Sci. 27 (1), 25–38. https://doi.org/10.1007/s11769-017-0844-3.

Tian, Y., Wang, S., Bai, X., Luo, G., Xu, Y., 2016. Trade-offs among ecosystem services in a typical Karst watershed, SW China. Sci. Total Environ. 566, 1297–1308. https://doi.org/10.1016/j.scitotenv.2016.05.190.

UNEP, 1997. World Atlas of Desertification. United Nations Environment Programme.

van der Velde, R., et al., 2014. Long term soil moisture mapping over the Tibetan plateau

using Special Sensor Microwave/Imager. Hydrol. Earth Syst. Sci. 18 (4), 1323–1337. https://doi.org/10.5194/hess-18-1323-2014.
Wang, D.J., Shen, Y.X., Huang, J., Li, Y.H., 2016. Rock outcrops redistribute water to nearby soil patches in karst landscapes. Environ. Sci. Pollut. Res. 23 (9), 8610–8616. https://doi.org/10.1007/s11356-016-6091-9.
Wang, Y., et al., 2018. Detecting the causal effect of soil moisture on precipitation using convergent cross mapping. Sci. Rep. 8. https://doi.org/10.1038/s41598-018-30669-2.
Wang, S.J., Liu, Q.M., Zhang, D.F., 2004. Karst rocky desertification in southwestern China: geomorphology, landuse, impact and rehabilitation. Land Degrad. Dev. 15 (2), 115–121. https://doi.org/10.1002/ldr.592.
Xia, Y., et al., 2014. Evaluation of multi-model simulated soil moisture in NLDAS-2. J. Hydrol. 512, 107–125. https://doi.org/10.1016/j.jhydrol.2014.02.027.
Xia, Y.Q., Shao, M.A., 2008. Soil water carrying capacity for vegetation: a hydrologic and biogeochemical process model solution. Ecol. Model. 214 (2–4), 112–124. https://doi.org/10.1016/j.ecolmodel.2008.01.024.
Xue, X., Guo, J., Han, B., Sun, Q., Liu, L., 2009. The effect of climate warming and permafrost thaw on desertification in the Qinghai-Tibetan Plateau. Geomorphology 108 (3–4), 182–190. https://doi.org/10.1016/j.geomorph.2009.01.004.
Yang, Y., et al., 2019. Factors affecting long-term trends in global NDVI. Forests 10 (5) 10.3390/f10050372.
Zhang, H., et al., 2015. Biogeographical patterns of forest biomass allocation vary by climate, soil and forest characteristics in China. Environ. Res. Lett. 10 (4). https://doi.org/10.1088/1748-9326/10/4/044014.
Zhang, Z.C., Chen, X., Shi, P., Ma, J.L., 2008. Influences of rock on soil moisture distribution in the karst cluster-peach mountains. Bull. Soil Water Conserv. 28 (6), 41–44.
Zhang, W., Zhou, T., Zhang, L., 2017. Wetting and greening Tibetan Plateau in early summer in recent decades. J. Geophys. Res.-Atmos. 122 (11), 5808–5822. https://doi.org/10.1002/2017jd026468.